Journal of Applied Polymer Science

Thermal, mechanical properties, and low-temperature performance of fibrous nanoclay-reinforced epoxy asphalt composites and their concretes

Yifan Sun,[1] Yuge Zhang,[1] Ke Xu,[1] Wei Xu,[2] Dier Yu,[3] Lei Zhu,[3] Hongfeng Xie,[1,3] Rongshi Cheng[1,4]

[1]Key Laboratory of High Performance Polymer Materials and Technology (Nanjing University), Ministry of Education, School of Chemistry and Chemical Engineering, Nanjing University, Nanjing 210093, China

[2]Road Engineering Institute, South China University of Technology, Guangzhou 510641, China

[3]National Engineering Laboratory for Advance Road Materials, Jiangsu Transportation Institute, Nanjing 211112, China

[4]College of Material Science and Engineering, South China University of Technology, Guangzhou 510641, China

Correspondence to: H. Xie (E-mail: hfxie@nju.edu.cn)

ABSTRACT: Epoxy asphalt (EA) concretes have been widely used in the pavement of orthotropic steel bridge decks. The objective of this study was to figure out the enhanced effects of natural fibrous attapulgite (ATT) as a reinforced nanofiller in ATT/EA nanocomposites through a comparison of the properties of the composites with a series of various nanoclay loadings. The rheological properties, glass transition, thermal stability, mechanical properties, and morphology of the ATT/EA composites were characterized. Furthermore, the low-temperature flexibility of the ATT/EA concretes was investigated. The test results show that the addition of ATT had no significant effect on the rotational viscosity of EA in the initial stage of the curing reaction. In addition, the ATT/EA composites showed better performance than the neat one in thermal stability with a higher glass-transformation temperature. The tensile strength and elongation at break of the ATT/EA composites at a loading of 0.5 wt % ATT were 21 and 22% higher than those of the neat EA. The addition of ATTs also enhanced the low-temperature flexibility of the EA concretes. © 2014 Wiley Periodicals, Inc. J. Appl. Polym. Sci. **2015**, *132*, 41694.

KEYWORDS: clay; composites; thermosets; thermogravimetric analysis; mechanical properties

Received 25 June 2014; accepted 30 October 2014

DOI: 10.1002/app.41694

INTRODUCTION

Asphalt, as a common thermoplastic, is widely used for paving roads all over the world because of its excellent viscoelastic properties in pavement construction. However, asphalt has some limitations. For example, it is very brittle at low temperatures, and it becomes liquid at high temperatures.[1] To overcome the limitations, polymers such as styrene–butadiene–styrene triblock copolymers,[2] rubber,[3] and ethylene–vinyl acetate copolymers,[4] have been used as additives for improving the properties of asphalts.[5]

The aforementioned polymer-modified asphalt cannot change the thermoplastic nature of asphalt; this means that asphalt flows easily at high temperatures. To change the thermoplastic properties of asphalt, thermosetting epoxy resin was incorporated into asphalt.[6] Asphalt modified with a thermosetting epoxy resin [epoxy asphalt (EA)] has excellent resistance to moisture damage, permanent deformation, and low-temperature cracking and is hence ideal for deck pavement in orthotropic steel deck bridges, especially in long-span steel bridges.[7] The San Mateo-Hayward Bridge built in 1967 was the first bridge in the world paved with EA concrete. Since then, EA concrete has been used widely in orthotropic steel deck pavements in Canada, Australia, and Brazil.[8] In China, EA concrete has been used in more than 40 long-span bridges since 2000. Furthermore, EA concrete has also been used in tunnels, pavement at intersections of heavy duty roads, and porous asphalt pavements with high durability.[9,10]

Nanoclays are widely used in the modification of polymer matrices to improve their mechanical, thermal, and barrier properties.[11,12] One of the most conventionally used nanoclays is montmorillonite (MMT), which has a 2:1 layered structure with two silica tetrahedrons sandwiching an alumina octahedron.[13] Attapulgite (ATT) is a type of natural fibrous nanoclay approximately 20–70 nm in diameter and several micrometers in length. Unlike other layered silicates, ATT consists of chains of a 2:1 phyllosilicate structure, and each of its ribbons is connected to the next by the inversion of SiO_4 tetrahedra along a

Table I. Aggregate Gradation for the ATT/EA Concretes

Sieve size (mm)	13.2	9.5	4.75	2.36	0.6	0.075
Percent passing (%)	100	95	68	60	33	10

set of Si—O—Si bonds and extends parallel to the *x* axis to form rectangular channels.[14–16] Because of their unique morphology and cheap price, much attention has been paid on ATT/polymer nanocomposites.[17–21] Chen *et al.*[19] found that the elastic modulus and yield strength of poly(ethylene terephthalate) were significantly improved by about 39.5% and 36.8%, respectively, by incorporating 2 wt % organically premodified ATT. Wang and Shen[20] reported that the strength and stiffness of polypropylene/*org*-ATT nanocomposites were both improved significantly in the presence of organic ATT. In addition, the incorporation of *org*-ATT also gave rise to an increase in the storage modulus (E') for polypropylene composites. We also studied silylated-ATT-reinforced soy polyol-based polyurethane (PU) previously.[22–24] 3-Glycidoxypropyltrimethoxysilane (GPTMS)-modified ATT increased the glass-transition temperature (T_g) and significantly improved the tensile strength and Young's modulus of the GPTMS–ATT/PU nanocomposites. Compared to the neat PU, the GPTMS–ATT/PU nanocomposite with 12 mass % GPTMS–ATT exhibited a 13.1°C increase in T_g, a 303% improvement in the tensile strength, and a 518% increase in the Young's modulus, respectively.[22] Recently, MMTs have been used to enhance the high-temperature storage stability, dynamic rheological and mechanical properties, and flame retardancy of the asphalts.[25–27] However, to our knowledge, few efforts have been made to study the effects of fibrous nanoclay on the physical properties of EA composite and its concrete. In this study, the fibrous ATT was incorporated into the EA composite as a nanofiller. To improve the ATT dispersion in the EA composite, a silane coupling agent was added. The structure and morphology of the modified ATT were determined. The rotational viscosity (RV), T_g, thermal stability, mechanical properties, and morphology of the ATT/EA composites were characterized. In addition, the low-temperature flexibility of the ATT-modified EA concrete was also evaluated.

EXPERIMENTAL

Materials

Base asphalt (AH-90 paving asphalt) was obtained from China Offshore Bitumen (Taizhou) Co., Ltd. (Taizhou, China). Diglycidyl ether of bisphenol A was supplied by Wuxi Resin Factory (Wuxi, China), of which the epoxy equivalent weight was 196 g/equiv. Modified acids (NDB2) provided by Nanjing Pureness Advanced Materials Co., Ltd. (China) were used as a curing agent. A silane coupling agent [γ-(2,3-epoxypropoxy) propytrimethoxysilane] was supplied by Trustchem Silanes Co., Ltd. (Nanjing, China). The raw ATT was obtained from the Jiangsu Golden Stone ATT R&D Co., Ltd. (Nanjing, China). The aggregate materials used were basalt, and the mineral filler was a graded limestone powder, all of which were obtained from Jiangsu Maodi Aggregates Co., Ltd. (China). Table I summarizes the aggregate gradation for the ATT/EA concretes used in this study. The optimum binder content of the ATT/EA concretes was chosen at 6.5% on the basis of the Marshall concrete design.

Preparation of the ATT/EA Composites

NDB2, asphalt, ATT, and KH560 were mixed with a JM-5 colloid mill at 120°C. Then, a certain amount of mixture and epoxy were stirred at 2000 rpm for 3 min in a 200 mL beaker. After the mechanical agitation, the mixtures were immediately poured into polytetrafluoroethylene molds and cured for 4 h at 120°C. The ATT loadings in the EA composites were 0, 0.5, 1, 3, and 5 wt %.

Test Methods

X-ray diffraction (XRD) study was carried out on a Shimadzu XRD-6000 with crystal monochromated Cu Kα radiation over the range $3° < 2\theta < 40°$ at a scanning rate of 6°/min.

The morphologies of the ATT and ATT/EA composites were observed by scanning electron microscopy (SEM; S-4800, Hitachi, Japan). The surface of the liquid-nitrogen-fractured samples was coated with gold before observation, and ATT powders were coated with gold before observation without liquid nitrogen.

A Brookfield rotational viscometer (model NDJ-1C, Shanghai Changji Instrument Co., Ltd., China) was used to evaluate the difference in viscous behavior between the EA and ATT/EA composites according to ASTM D 4402. The RV tests were conducted at 120°C.

The T_gs of the ATT/EA composites were studied by dynamic mechanical analysis (DMA; DMA+450, 01dB-Metravib, France). The measurements were performed from −50 to 80°C under tension mode at a heating rate of 2°C/min and a frequency of 1 Hz.

Thermogravimetric analysis (TGA) was measured with a PerkinElmer Pyris 1 TGA instrument at a 20°C/min heating rate under a nitrogen atmosphere with a temperature range (ΔT) of 25–600°C.

The tensile properties were examined with a universal testing machine (Instron 4466) with a strain rate of 500 mm/min at 23°C by 500 N according to the standard of ASTM D 638. An Instron model 4466 was used to cut a sample 15 × 5 × 2 mm^3 (Specimen gauge length × Width × Thickness). The results were averaged over at least six specimens.

Three-point bending beam tests were carried out at a loading rate of 50 mm/min at −15°C to determine the low-temperature flexibility of the ATT/EA concretes according to JTJ 052–2000 of China. A sample (300 × 300 × 50 mm^3) was first compacted with a wheel-tracking compactor and was then cut into four beams (250 × 30 × 35 mm^3). These samples were put into a constant-temperature chamber, which was cooled to −15°C by a recycled methanol aqueous solution (1:1). Three of the four samples were selected randomly as specimens for the three-point bending test after they were cooled at −15°C for 1 h.

RESULTS AND DISCUSSION

XRD

Figure 1 shows the XRD patterns of the neat ATT and ATT/EA composites. A typical diffraction peak of the neat ATT was at

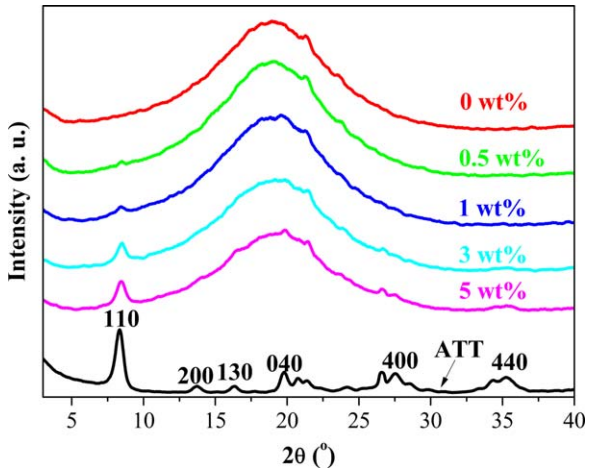

Figure 1. XRD patterns of the neat ATT and ATT/EA composites. [Color figure can be viewed in the online issue, which is available at wileyonlinelibrary.com.]

about 8.4°; this corresponded to a basal spacing of about 1.04 nm and could be assigned to the primary diffraction of the (110) crystal face.[28] Unlike the structure of MMT, for ATT, the characteristic diffraction peak (110) was due to the intrinsic axis structure of rodlike crystals. The mix of ATT and EA could not shift the structure of these rodlike crystals, so the position of this characteristic peak was not changed when ATT separated.[29] The same result was justified by Yuan *et al.*[30] in a similar system. Therefore, this peak could be considered a characteristic peak for identifying the separation of ATT in the matrix. As shown in Figure 1, the ATT/EA composites showed a weak characteristic peak of ATT at 8.4°. With increasing ATT content for the nanocomposites, the intensity of the peak at $2\theta = 8.4°$ was enhanced; this showed that asphalt did not strongly affect ATT's rodlike crystal construction. Moreover, both the neat EA and ATT/EA composites showed a broad peak around $2\theta = 18.8°$; this indicated that the morphology of the EA composite was essentially noncrystalline. Also, the addition of the ATTs did not change the crystal structure of EA. Similar results were also reported for ATT-modified epoxy/PU interpenetrating networks.[15] So, ATT had no interaction with asphalt during the curing reaction.

Morphology

The morphology of the ATTs in the EA composites was examined with SEM. As shown in Figure 2(a), the ATT exhibited a uniform fibrous shape and had a length of several micrometers and the smallest diameter of approximately 30 nm (a single ATT crystal). Figure 2(b–f) shows low-magnification SEM images of the fractured surface morphologies of the neat EA and ATT/EA composites. Evidently, phase separation appeared in the EA composites; that is, the asphalts with evenly spherical particles were distributed in the sea of the epoxy matrix. The asphalt spherical particles were suspected to cause some localized plastic shear yielding, which resulted in the observed increase in the toughness of the epoxy resin.[31,32] Similar phase separations were also found in the asphalt-modified epoxy materials.[33–35] As shown in Figure 2(c,d), the ATTs appeared as bright points (the ends of broken ATTs) and were dispersed uniformly in the EA composites at lower loadings in the micrographs. However, the ATTs tended to form irreversible agglomerates at higher loadings [as shown in Figures 2(e,f) and 3(a,b)] because of their high specific surface areas, hydrogen bonding, and intrinsic van der Waal's interactions. These agglomerates had disadvantageous effects on the properties of the ATT/EA composites, as discussed later.

RV

Unlike asphalt, EA is a thermosetting material. This means that EA's RV would increase during the curing reaction. Therefore, the mixing time was carefully controlled to give a uniform coating of EA on all of the aggregates. The RV–time plots of the EA and ATT/EA composites are shown in Figure 4. Noticeably, the ATT had no significant effect on the RV of EA in the initial stage of the curing reaction. The results were different than those of other nanoclay-modified epoxy resin and asphalts, whose RV increased greatly with increasing nanoclay loadings.[36–39] It is known that ATT suspensions are thixotropic and non-Newtonian at all concentrations.[40] They exhibit a rapid increase in fluidity as the shear separates the individual nanorods, which are held together in bundles by electrostatic forces. Without sufficient shear force, ATT does not disperse well. In this study, a colloid mill was used to disperse the ATTs in the EA. Hence, the low viscosity of the ATT/EA composites was attributed to the thixotropy of ATTs. Similar results were also reported for a polyacrylonitrile/ATT solution.[41] According to Strategic Highway Research Program specifications, RV should be below 3 Pa s for compacting concrete. If the RV of EA exceeds 3 Pa·s, it becomes very hard for the concrete to compact the pavement, and eventually, it becomes difficult for an eligible pavement surface to form.[42] As shown in Figure 4, the time to 3 Pa s for the ATT/EA composites increased with ATT loading; this indicated that ATT slightly hindered the curing reaction of EA in the later stage.

Dynamic Mechanical Properties

DMA is often used to study relaxation in polymers. An analysis of the E', loss modulus, and loss factor (tan δ) curves was very useful for ascertaining the performance of samples under stress and temperature. The E' and tan δ versus temperature curves for the neat EA and ATT/EA composites are presented in Figure 5. The E' values at −30 and 25°C for the neat EA and ATT/EA composites are listed in Table II. The E's of the ATT/EA composites increased with increasing ATT loading. The E' of the ATT/EA composites was greater than that of the neat EA at lower temperature (−30°C) but lower than that of the neat EA composite at the temperature near T_g (25°C), except for at the 5 wt % ATT loading. The T_g of the ATT/EA composites was determined by the peak position of tan δ. We found that the T_gs of the ATT/EA composites were lower than that of the neat EA (25.6°C). Moreover, the T_g of the ATT/EA composites increased with increasing ATT loading. These phenomena were similar to the relaxation behaviors of other nanocomposites reported previously.[19,43–48] In this study, the T_g decrease of the ATT/EA composites was due to the crosslinking density reduction effect of ATT because the ATT hindered the curing reaction of the EA composite, as most references about clay-modified nanocomposites have reported.[49] Similar results were also found in ATT-modified epoxy nanocomposites.[19] Meanwhile, when ATT

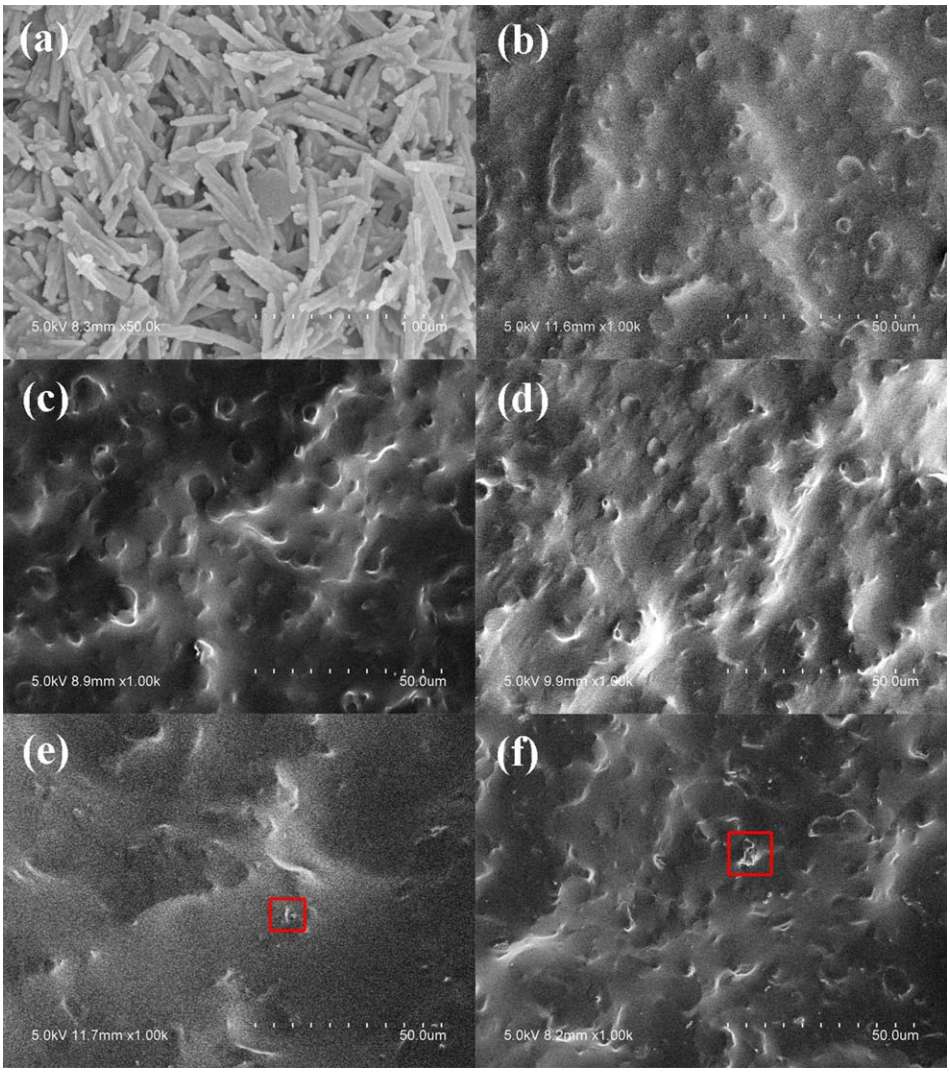

Figure 2. SEM images of the (a) neat ATT and ATT/EA composites with different ATT loadings: (b) 0, (c) 0.5, (d) 1, (e) 3, and (f) 5 wt %. [Color figure can be viewed in the online issue, which is available at wileyonlinelibrary.com.]

increased, the confined environment restricted the mobility of polymer chains.[50] As a result, the EA segments were more mobile in low-ATT-content ATT/EA composites than in the high-ATT-content ATT/EA composites; this led to the T_g increase in the ATT/EA composites. As shown in Figure 5(b), each tan δ curve also displays an inconspicuous peak around $-10°C$; this accounted for the β transition of asphalt.[51] Similar results were reported by Wise *et al.*[52] for carboxyl-terminated butadiene-acrylonitrile (CTBN) rubber phase precipitation in epoxy resins.

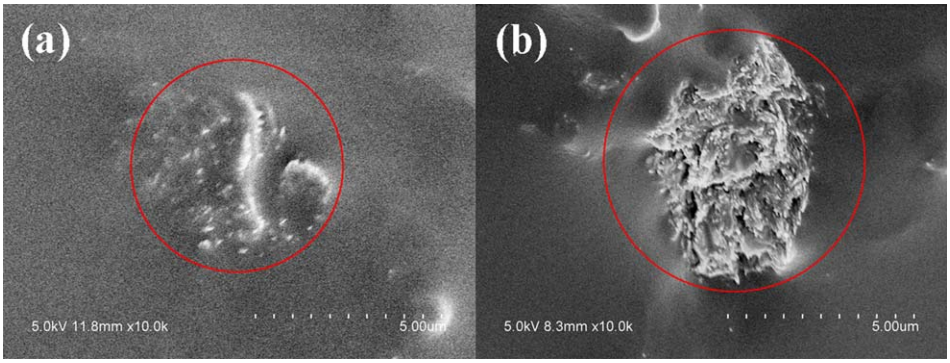

Figure 3. Magnified SEM images of the ATT/EA composites with different ATT loadings: (a) 3 and (b) 5 wt %. [Color figure can be viewed in the online issue, which is available at wileyonlinelibrary.com.]

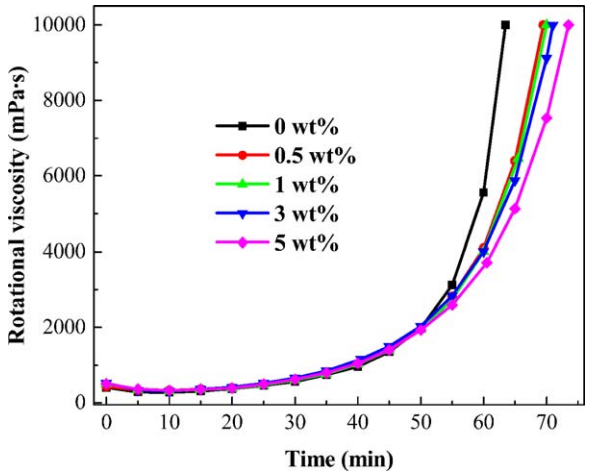

Figure 4. RV–time plots for the neat EA and ATT/EA composites at 120°C. [Color figure can be viewed in the online issue, which is available at wileyonlinelibrary.com.]

Tan δ, which indicates the relaxation behavior and damping ability of the material, is the ratio of the mechanical dissipation energy to the storage energy. In comparison to the neat EA, the ATT/EA composites showed a higher magnitude of tan δ at the tan δ peak. It was reported that a composite material with poor interfacial bonding between the fibers and matrix would tend to dissipate more energy and show a high magnitude of the damping peak in comparison to a material with a strongly bonded interface.[53] Therefore, we concluded that the interface of ATT had no strong interaction with asphalt; this was substantiated by our XRD results.

Polymer-modified asphalt, which has a higher tan δ intensity, is often used as a viscoelastic damping material on noise and vibration reduction within railway vehicles.[47] In this study, the damping behavior of ATT-modified EA was quantitatively evaluated by the loss tangent maximum [$(\tan\delta)_{max}$], ΔT for efficient damping (tan $\delta > 0.3$), and the area under the tan δ versus temperature curve (TA).[47,52] All of these parameters for the neat EA and ATT/EA composites are listed in Table II. The $(\tan\delta)_{max}$ of the neat EA composite was 1.52; this was much higher than that of the common polymer or polymer composites (<0.3). The addition of ATT increased the $(\tan\delta)_{max}$ of the neat EA. The EA composite with 1 wt % ATT had the highest $(\tan\delta)_{max}$ value (1.60). The efficient damping (tan $\delta > 0.30$) and TA value of the neat EA composite were over a narrow ΔT from 10.10 to 46.65°C ($\Delta T = 35.55$°C) and a low TA value (36.49 K). The addition of ATTs increased ΔT and TA of the neat EA composite. The ATT/EA composites with 0.5 and 1 wt % ATT loadings had the greatest ΔT and TA values, which were 40.10 and 41.18 K, respectively; this was attributed to the better dispersion of the ATTs in the EA composites, as discussed previously. Overall, the addition of natural fibrous nanoclay slightly improved the damping properties of the EA composite.

Thermal Stability

TGA and derivative thermogravimetry (DTG) plots of the neat EA and ATT/EA composites are shown in Figure 6. The EA we used normally exhibits one-stage degradation during heating; ATT did not significantly change the main profile of the TGA curves for the matrix. The initial decomposition temperature (IDT), which was set as the temperature when 5% mass was lost, the residue at 600°C, and the maximum degradation temperatures (T_{max}'s) of the samples are summarized in Table III. We observed that the IDTs and T_{max} values of the ATT/EA composites were higher than those of the neat EA; this indicated that the addition of ATTs enhanced the thermal stability of EA. Furthermore, the IDTs and T_{max} values increased with increasing ATT loading and reached the maximal value at a loading of 3 wt %, respectively, 28.6 and 25.8°C higher than those of the neat EA (347.0 and 459.3°C). When the ATT loading was above 3 wt %, both IDT and T_{max} decreased slightly. It is known that nanoclay particles have a significant barrier effect to slow down products' volatilization and thermal transport during the decomposition of polymers; this endowed the composites with a high thermal stability. Simultaneously, the adsorption of polymer chains onto the surface of the well-dispersed clay restricted of segmental mobility and suppressed the redistribution and chain-transfer reactions. However, metal ions and derivatives exchanged or adsorbed into clay crystal interspaces, played a

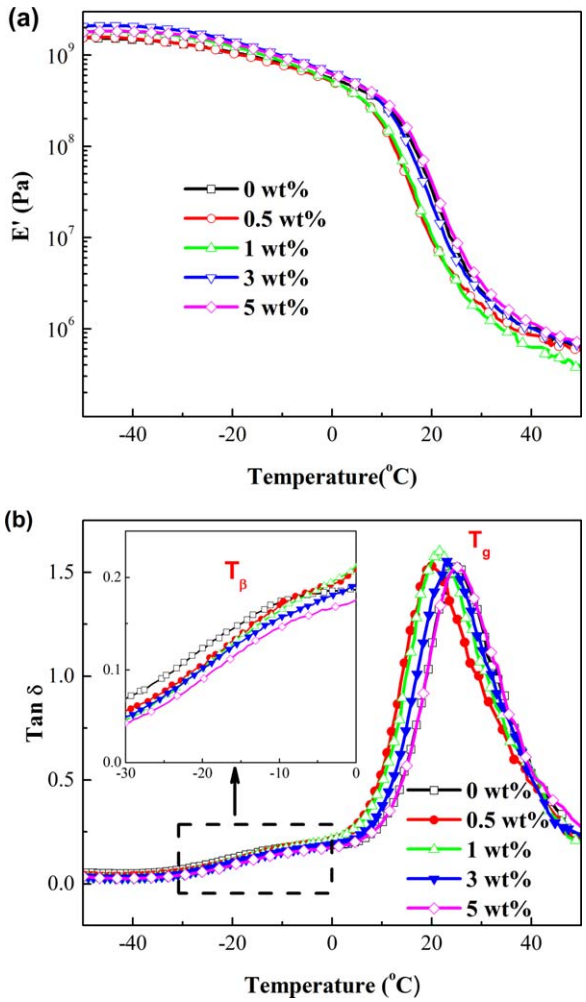

Figure 5. Dynamic mechanical properties of the neat EA and ATT/EA composites: (a) E' and (b) tan δ. [Color figure can be viewed in the online issue, which is available at wileyonlinelibrary.com.]

Table II. E' and T_g Values and Damping Properties of the Neat EA and ATT/EA Composites

	E'						
ATT (wt %)	−30°C (GPa)	25°C (MPa)	T_g (°C)	T_β (°C)	$(\tan\delta)_{max}$	ΔT at $\tan\delta > 0.3$	TA (K)
0	1.33	7.37	25.6	−9.75	1.52	35.55 (10.10-46.65)	36.49
0.5	1.33	3.27	20.0	−11.10	1.53	40.10 (5.90-46.00)	38.67
1	1.62	3.41	21.6	−8.70	1.60	39.80 (6.35-46.15)	41.18
3	1.84	5.63	23.1	−11.45	1.55	36.60 (8.15-44.75)	38.15
5	1.66	8.64	25.1	−8.40	1.53	38.15 (9.90-48.05)	38.60

T_β: the temperature of the β transition of asphalt
The initial and final temperatures for $\tan\delta > 0.3$.

principal accelerating role in the decomposition of the polymer chains.[54] Therefore, the thermal degradation of the ATT/EA composites was due to the coexistence of a barrier effect and metal-ion catalytic decomposition. In this study, the addition of ATT in the EA matrix formed barriers that enhanced the thermal stability, and the barrier effect was dominant at low ATT loadings. However, at the 5 wt % ATT loading, too many metal ions and derivatives exchanged or adsorbed into the clay–crystal interspaces partly counteracted the barrier effect of the ATTs. Meanwhile, the ATTs began to agglomerate, as the SEM images show [Figure 2(e,f)]; this weakened the barrier effect. That was why both the IDT and T_{max} decreased slightly when the ATT loading was greater than 3 wt %. As shown in Table III, the residue at 600°C of the ATT/EA composites increased with increasing ATT loading. Because of the covalent bonding with matrix, the residue of the ATT/EA composites was lower than that of the neat EA at lower ATT loadings.

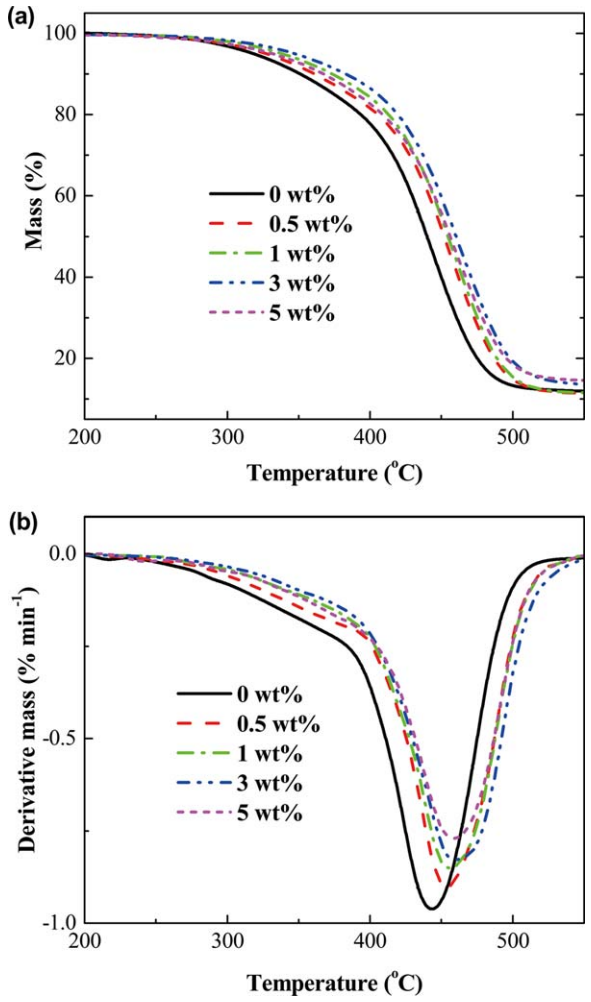

Figure 6. (a) TGA and (b) DTG plots for the neat EA and ATT/EA composites. [Color figure can be viewed in the online issue, which is available at wileyonlinelibrary.com.]

Mechanical Properties

The results of the tensile tests are presented in Figures 7 and 8. Figure 7 is the load–displacement curves, and Figure 8 shows the tensile strength and elongation at break of the ATT/EA composites as a function of the ATT loading. As shown in Figure 7, a tough fracture was evident for the neat EA and ATT/EA composites with a yield point, whereas the appearance of the yield point was put off with higher yield stress values with the addition of ATTs. Also, the samples with various ATT contents displayed very similar brittle–ductile behavior, as observed from these curves; this indicated that the structure of EA was not changed by the addition of ATTs. Meanwhile, as shown in Figure 8, the tensile strength and elongation at break of the ATT/EA composites were higher than those of the neat EA and had the highest value (5.84 MPa and 485%) at a loading of 0.5 wt % ATT and were 21 and 22%, respectively, higher than those of the neat EA (4.84 MPa and 397%). Generally, the tensile strength improvement was apt to be accompanied by a sacrifice in the toughness. However, in our case, the addition of ATT to the EA improved both the strength and toughness. Similar results were reported for other ATT/polymer composites.[55–57]

Table III. TGA and DTG Results of the Neat EA and ATT/EA Composites

ATT (wt %)	IDT (°C)	Residue at 600°C (%)	T_{max} (°C)
0	318.4	11.5	433.5
0.5	327.2	10.9	453.9
1	338.4	11.1	455.8
3	347.0	13.1	459.3
5	331.4	14.2	458.5

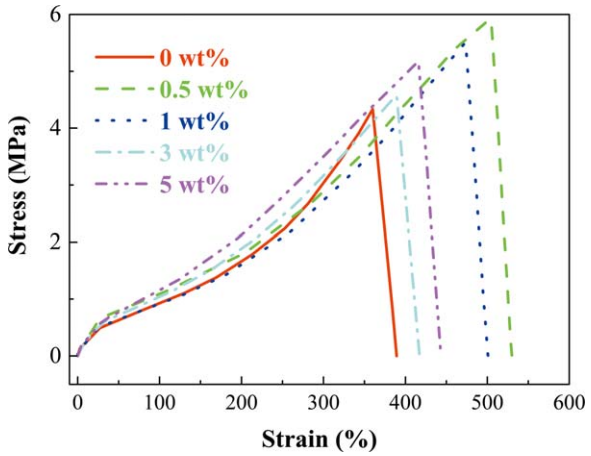

Figure 7. Stress–strain curves of the neat EA and ATT/EA composites with different ATT loadings. [Color figure can be viewed in the online issue, which is available at wileyonlinelibrary.com.]

Wang *et al.*[20] showed that the nonmetric dispersion of ATT in the polymer matrix led to the improved modulus and strength. In this study, the tensile strength and toughness increase in the presence of ATT also directly benefitted from the reinforcement provided by the well-dispersed ATT interfacial interaction between ATT and EA.[55,57] As for the high-ATT-loading composites, the formation of agglomerates, as the SEM images show [Figure 2(e,f)], resulted in the fact that the ATTs could not act efficiently to dissipate the mechanical energy and instead served as flaws or defects and crack-initiation sites.[58] So the tensile strength and toughness decreased to some extent for the 3 and 5 wt % samples.

Low-Temperature Flexibility

The results of the three-point bending beam test are given in Figure 9 and Table IV. The force–displacement curves illustrated in Figure 9 were similar to straight lines and had approximate absolute values with each other. That the structure of EA was not changed by the addition of ATT was verified again by the three-point bending beam test. As observed, the critical strain (ε_c) and critical stress (σ_c) of the ATT/EA concretes were slightly

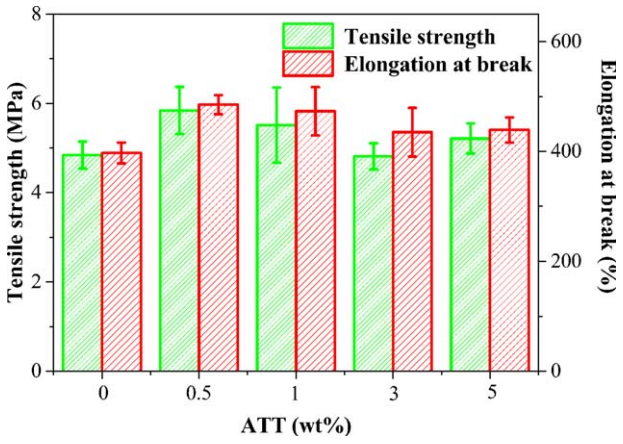

Figure 8. (a) Tensile strength and (b) elongation at break for the neat EA and ATT/EA composites. [Color figure can be viewed in the online issue, which is available at wileyonlinelibrary.com.]

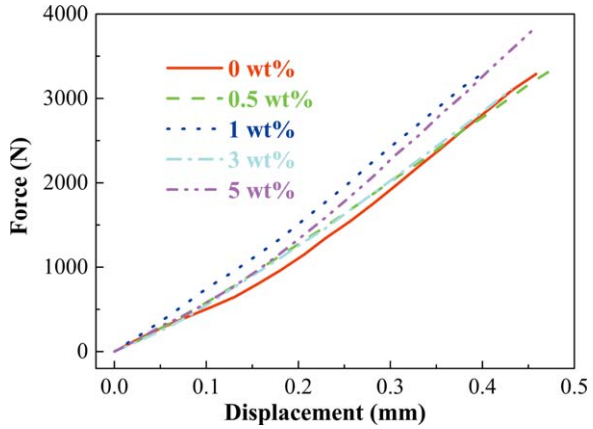

Figure 9. Force–displacement curves from the three-point bending beam test. [Color figure can be viewed in the online issue, which is available at wileyonlinelibrary.com.]

greater than those of the neat EA concrete; this showed that the positive effect of ATTs on the resistance of the EA concrete to cracking at low-temperature. Therefore, we concluded that the addition of nature fibrous nanoclay helped to improve the low-temperature flexibility of EA concrete.

The bending stiffness modulus (S_c; MPa) was an important test result obtained from the three-point bending beam test, which showed the stiffness of asphalt concrete at low temperature. S_c, calculated by eq. (1), is listed in Table IV. As shown, the ATTs had no influence on the stiffness of the EA concretes when the ATT loading was lower than 3 wt %. The EA concrete with 5 wt % ATT had the lowest S_c; this was attributed to the agglomeration of ATTs in the EA composites, as motioned previously.

$$S_c = \frac{\sigma_c}{\varepsilon_c} \times 10^6 \tag{1}$$

The area below the strain–stress curve of the asphalt concrete was the bending strain energy density. The critical bending strain energy density (G_f^c) was the absorbed energy per unit projected area of the fracture zone during the complete fracture process.[59] The relevant equation is shown as follows:

$$G_f^c = \int_0^{\varepsilon_c} \sigma d\varepsilon \tag{2}$$

where σ is the stress fraction and ε is the strain fraction.

The greater the bending strain energy density was, the better the low-temperature performance was. The G_f^c values of the EA concrete and ATT/EA concretes are presented in Table IV.

Table IV. Three-Point Bending Beam Test Results of the Neat EA and ATT/EA Concretes

ATT (wt %)	σ_c (MPa)	ε_c ($\mu\varepsilon$)	S_c (MPa)	G_f^c (J/m^3)
0	29.2	2159	13,632	2508
0.5	31.7	2348	13,527	3020
1	31.6	2027	15,628	2586
3	31.1	2314	13,490	2779
5	29.5	2383	12,563	2741

Obviously, the G_f^c of the ATT/EA concrete was higher than that of the neat EA concrete; this indicated that the addition of ATT improved the low-temperature flexibility of the EA concrete. The EA concrete with 0.5 wt % ATT had the greatest G_f^c value; it was 20% higher than that of the neat EA concrete and showed great resistance to cracking at low temperature.

CONCLUSIONS

In this study, we investigated the influence of fibrous nanoclay (ATT) on the morphology, RV, T_g, thermal stability, mechanical properties, and low-temperature flexibility of the EA composite and its concrete. The conclusions of this study were as follows:

- The addition of ATT had no significant effect on the viscosity of EA in the initial stage and slightly hindered the curing reaction in the later stage.
- The DMA results show that the T_g of the ATT/EA composite was lower than that of the neat EA and increased with increasing ATT loading.
- TGA demonstrated that the addition of ATT improved the thermal stability of EA. The IDT and T_{max} values of the 3 wt % ATT/EA composite were 28.6 and 25.8°C higher than those of the neat EA.
- The tensile tests show that the strength and toughness of the EA improved with the addition of the ATTs. Compared with the neat EA, the tensile strength and elongation at break of ATT/EA composites at a loading of 0.5 wt % ATT increased by 21 and 22%, respectively.
- The three-point bending beam test showed that the addition of ATT improved the low-temperature flexibility of the EA concretes and made a contribution to overcome the brittleness at low temperature.

ACKNOWLEDGMENTS

The authors are grateful for financial support from the Opening Funds of National Engineering Laboratory for Advance Road Materials, Jiangsu Province Natural Science Foundation (contract grant number BK2011085), the Program for Changjiang Scholars and Innovative Research Team in University, and the Fundamental Research Funds for the Central Universities (contract grant number 20620140066). The authors are also grateful to Sunjie Ye and Laiqiang Ying for language help.

REFERENCES

1. Zhang, L. Q.; Greenfield, M. L. *Energy Fuels* **2008**, *22*, 3363.
2. Adedeji, A.; Grunfelder, T.; Bates, F. S.; Macosko, C. W.; StroupGardiner, M.; Newcomb, D. E. *Polym. Eng. Sci.* **1996**, *36*, 1707.
3. Mull, M. A.; Stuart, K.; Yehia, A. J. *Mater. Sci.* **2002**, *37*, 557.
4. Gonzalez, O.; Munoz, M. E.; Santamaria, A.; Garcia-Morales, M.; Navarro, F. J.; Partal, P. *Eur. Polym. J.* **2004**, *40*, 2365.
5. Yildirim, Y. *Construction Building Mater.* **2007**, *21*, 66.
6. Cubuk, M.; Guru, M.; Cubuk, M. K. *Fuel* **2009**, *88*, 1324.
7. Qian, J. S.; Wang, Q. Z.; Wu, W. J.; Zhang, H. *Mater. Des.* **2013**, *52*, 686.
8. Gaul, R. In New Technologies in Construction and Rehabilitation of Portland Cement Concrete Pavement and Bridge Deck Pavement; Moon, W., Yoon, H. C., Shiraz, T., Yuan, J. B., Eds.; Geotechnical Special Publications: Reston, 2009; p 196.
9. Kang, Y.; Chen, Z. M.; Jiao, Z.; Huang, W. *J. Appl. Polym. Sci.* **2010**, *116*, 1678.
10. Qian, Z. D.; Chen, L. L.; Jiang, C. L.; Luo, S. *Construction Building Mater.* **2011**, *25*, 3117.
11. Alateyah, A. I.; Dhakal, H. N.; Zhang, Z. Y. *Adv. Polym. Technol.* **2013**, *32*, 36.
12. Zhu, L. X.; Liu, P.; Wang, A. Q. *Ind. Eng. Chem. Res.* **2014**, *53*, 2067.
13. Greesh, N.; Ray, S. S.; Bandyopadhyay, J. *Ind. Eng. Chem. Res.* **2013**, *52*, 16220.
14. Bradley, W. F. *Am. Mineralog.* **1940**, *25*, 405.
15. Lei, Z. Q.; Yang, Q. L.; Wu, S.; Song, X. L. *J. Appl. Polym. Sci.* **2009**, *111*, 3150.
16. Lu, H. B.; Shen, H. B.; Song, Z. L.; Shing, K. S.; Tao, W.; Nutt, S. *Macromol. Rapid Commun.* **2005**, *26*, 1445.
17. Zhang, Y.; Shen, J.; Li, Q.; Pang, L.; Zhang, Q. Y.; Xu, Z. S.; Yeung, K. W. K.; Yi, C. F. *Compos. A* **2013**, *55*, 161.
18. Xue, S. Q.; Reinholdt, M.; Pinnavaia, T. J. *Polymer* **2006**, *47*, 3344.
19. Chen, L.; Liu, K.; Jin, T. X.; Chen, F.; Fu, Q. *Express Polym. Lett.* **2012**, *6*, 629.
20. Wang, L.; Sheng, J. *Polymer* **2005**, *46*, 6243.
21. Wang, R. G.; Li, Z.; Wang, Y. M.; Liu, W. B.; Deng, L. B.; Jiao, W. C.; Yang, F. *Polym. Compos.* **2013**, *34*, 22.
22. Wang, C. S.; Wu, Q. S.; Liu, F.; An, J.; Lu, R.; Xie, H. F.; Cheng, R. S. *Appl. Clay Sci.* **2014**, *101*, 246.
23. Wang, C. S.; Wang, Y. T.; Liu, W. J.; Yin, H. Y.; Yuan, Z. R.; Wang, Q. J.; Xie, H. F.; Cheng, R. S. *Mater. Lett.* **2012**, *78*, 85.
24. Wang, C. S.; Ding, L.; Wu, Q. S.; Liu, F.; Wei, J.; Lu, R.; Xie, H. F.; Cheng, R. S. *Ind. Crops Prod.* **2014**, *57*, 29.
25. Galooyak, S. S.; Dabir, B.; Nazarbeygi, A. E.; Moeini, A.; Berahman, B. *Pet. Sci. Technol.* **2011**, *29*, 850.
26. Jahromi, S. G.; Khodaii, A. *Construction Building Mater.* **2009**, *23*, 2894.
27. Bonati, A.; Merusi, F.; Bochicchio, G.; Tessadri, B.; Polacco, G.; Filippi, S.; Giuliani, F. *Construction Building Mater.* **2013**, *47*, 990.
28. Pan, B. L.; Yue, Q. F.; Ren, J. F.; Wang, H. G.; Jian, L. Q.; Zhang, J. Y.; Yang, S. R. *Polym. Test.* **2006**, *25*, 384.
29. Tian, M.; Qu, C. D.; Feng, Y. X.; Zhang, L. Q. *J. Mater. Sci.* **2003**, *38*, 4917.
30. Yuan, X.; Li, C.; Guan, G.; Liu, X.; Mao, Y.; Zhang, D. *J. Appl. Polym. Sci.* **2007**, *103*, 1279.
31. Chikhi, N.; Fellahi, S.; Bakar, M. *Eur. Polym. J.* **2002**, *38*, 251.

32. Wang, Y. T.; Wang, C. S.; Yin, H. Y.; Wang, L. L.; Xie, H. F.; Cheng, R. S. *Express Polym. Lett.* **2012**, *6*, 719.
33. Yin, H. Y.; Jin, H.; Wang, C. S.; Sun, Y. F.; Yuan, Z. R.; Xie, H. F.; Wang, Z. L.; Cheng, R. S. *J. Therm. Anal. Calorim.* **2014**, *115*, 1073.
34. Wang, Y. P.; Ye, J. F.; Liu, Y. H.; Qiang, X. H.; Feng, L. B. *Construction Building Mater.* **2013**, *41*, 580.
35. Yin, H. Y.; Zhang, Y. G.; Sun, Y. F.; Xu, W.; Yu, D. E.; Xie, H. F.; Cheng, R. S. *Mater. Struct.* **2014**, DOI: 10.1617/s11527-014-0442-0.
36. Xu, Y.; Van Hoa, S. *Compos. Sci. Technol.* **2008**, *68*, 854.
37. Mohan, T. P.; Kumar, M. R.; Velmurugan, R. *Polym. Int.* **2005**, *54*, 1653.
38. Galooyak, S. S.; Dabir, B.; Nazarbeygi, A. E.; Moeini, A. *Construction Building Mater.* **2010**, *24*, 300.
39. You, Z. P.; Mills-Beale, J.; Foley, J. M.; Roy, S.; Odegard, G. M.; Dai, Q. L.; Goh, S. W. *Construction Building Mater.* **2011**, *25*, 1072.
40. Haden, W. L.; Schwint, I. A. *Ind. Eng. Chem.* **1967**, *59*, 58.
41. Yin, H.; Mo, D.; Chen, D. *J. Polym. Sci. Part B: Polym. Phys.* **2009**, *47*, 945.
42. Yu, J. Y.; Cong, P. L.; Wu, S. P. *J. Appl. Polym. Sci.* **2009**, *113*, 3557.
43. Xie, H. F.; Liu, B. H.; Yang, H.; Wang, Z. L.; Shen, J. Y.; Cheng, R. S. *J. Appl. Polym. Sci.* **2006**, *100*, 295.
44. Xie, H. F.; Liu, C. G.; Yuan, Z. R.; Yang, H.; Wang, Z. L.; Cheng, R. S. *Acta Polym. Sinica* **2008**, *4*, 332.
45. Wang, C. S.; Chen, X. Y.; Xie, H. F.; Cheng, R. S. *Compos. A* **2011**, *42*, 1620.
46. Chen, S. B.; Wang, Q. H.; Wang, T. M.; Pei, X. Q. *Mater. Des.* **2011**, *32*, 803.
47. Zhang, J. S.; Wang, Y. T.; Wang, X. S.; Ding, G. W.; Pan, Y. Q.; Xie, H. F.; Chen, Q. M.; Cheng, R. S. *J. Appl. Polym. Sci.* **2014**, *131*, 40472.
48. Zhang, Y. G.; Pan, X. Y.; Sun, Y. F.; Xu, W.; Pan, Y. Q.; Xie, H. F.; Cheng, R. S. *Construction Building Mater.* **2014**, *68*, 62.
49. Wu, Z. G.; Zhou, C. X.; Qi, R. R.; Zhang, H. B. *J. Appl. Polym. Sci.* **2002**, *83*, 2403.
50. Wan, C. Y.; Qiao, X. Y.; Zhang, Y.; Zhang, Y. X. *Polym. Test.* **2003**, *22*, 453.
51. Qi, Z. G.; Ye, H. M.; Xu, J.; Chen, J. N.; Guo, B. H. *Colloids Surf. A* **2013**, *421*, 109.
52. Wise, C. W.; Cook, W. D.; Goodwin, A. A. *Polymer* **2000**, *41*, 4625.
53. Mohanty, S.; Verma, S. K.; Nayak, S. K. *Compos. Sci. Technol.* **2006**, *66*, 538.
54. Yuan, X. P.; Li, C. C.; Guan, G. H.; Xiao, Y. N.; Zhang, D. *Polym. Degrad. Stab.* **2008**, *93*, 466.
55. Wang, C. S.; Chen, X. Y.; Chen, J. Q.; Liu, C. G.; Xie, H. F.; Cheng, R. S. *J. Appl. Polym. Sci.* **2011**, *122*, 2449.
56. Jin, H.; Zhang, Y. G.; Wang, C. S.; Sun, Y. F.; Yuan, Z. R.; Pan, Y. Q.; Xie, H. F.; Cheng, R. S. *J. Therm. Anal. Calorim.* **2014**, *117*, 773.
57. An, L.; Pan, Y. Z.; Shen, X. W.; Lu, H. B.; Yang, Y. L. *J. Mater. Chem.* **2008**, *18*, 4928.
58. Prabhu, T. N.; Demappa, T. *J. Appl. Polym. Sci.* **2014**, *131*, 7.
59. Ni, P.; Li, J.; Suo, J. S.; Li, S. B. *J. Mater. Sci.* **2004**, *39*, 4671.